

# FisheyeDistill: Self-Supervised Monocular Depth Estimation with Ordinal Distillation for Fisheye Cameras

Qingan Yan<sup>1</sup>  
qingan.yan@innopeaktech.com

Pan Ji\*<sup>13</sup>  
pan.ji@innopeaktech.com

Nitin Bansal<sup>1</sup>  
nitin.bansal@innopeaktech.com

Yuxin Ma<sup>†2</sup>  
yuxinma2005@gmail.com

Yuan Tian<sup>1</sup>  
yuan.tian@innopeaktech.com

Yi Xu<sup>1</sup>  
yi.xu@innopeaktech.com

<sup>1</sup>OPPO US Research Center  
InnoPeak Technology, Inc.  
Palo Alto, California, US

<sup>2</sup>Wing LLC  
Mountain View, California, US  
(<sup>†</sup>Work done while at OPPO US Research Center.)

<sup>3</sup>\*Corresponding author

## Abstract

In this paper, we deal with the problem of monocular depth estimation for fisheye cameras in a self-supervised manner. A known issue of self-supervised depth estimation is that it suffers in low-light/over-exposure conditions and in large homogeneous regions. To tackle this issue, we propose a novel ordinal distillation loss that distills the ordinal information from a large teacher model. Such a teacher model, since having been trained on a large amount of diverse data, can capture the depth ordering information well, but lacks in preserving accurate scene geometry. Combined with self-supervised losses, we show that our model can not only generate reasonable depth maps in challenging environments but also better recover the scene geometry. We further leverage the fisheye cameras of an AR-Glasses device to collect an indoor dataset to facilitate evaluation.

## 1 Introduction

Fisheye cameras have gradually gained popularity on Head Mounted Display (HMD), as it offers a large field-of-view (FoV) that is well suited for immersive AR/VR experience. To estimate the depth map from a distorted fisheye image, a typical prerequisite is to perform image rectification. Such a rectification step, however, undermines the benefits of using fisheye cameras because it will inevitably reduce the FoV of the camera. Moreover, image rectification itself is expensive on HMD as there are only very limited computational resources available on the device. Therefore, it's desirable to directly estimate a depth map from the fisheye image, which is the main theme of this paper.

The past few years have seen a growing interests in self-supervised depth estimation [1, 11, 40] because it requires no groundtruth depth during training and yet achieves comparable results with some of the well known supervised methods. However, due to dearth of effective benchmarking datasets, depth estimation for fisheye cameras remains under-explored, with only a few exceptions [18, 19]. Nonetheless, those fisheye depth estimation methods [18, 19] are only evaluated on well-conditioned outdoor self-driving datasets, including the WoodScape dataset [58], for which the groundtruth depths are not yet publicly available. In this work, we follow this trend to take a self-supervised approach to estimating a depth map from a distorted image, but under a more challenging environment, which is captured by HMD.

Self-supervised depth estimation is not without challenges because the key supervision signal of photo-consistency can become ineffective in low-light/over-exposure conditions and in large areas of no/little textures as commonly seen in indoor environments. On the other hand, there has been depth models that are trained on a variety of datasets and can generalize well to new unseen domains [27, 28, 36]. Although such depth models can generate visually good-looking depth maps, the 3D scene geometry in those depth maps are often not well recovered [36]. For example, when visualizing the depth maps of an indoor room in 3D, the horizontal and vertical walls may not be perpendicular to each other, showing distorted 3D scene geometry [36].

In this work, we propose to combine the best of self-supervised depth estimation and knowledge distillation [13] to build a robust depth model for fisheye cameras especially in challenging indoor environments. In particular, we adapt the photometric loss [10], which is usually based on a pin-hole camera model, to a fisheye camera model. On top of the self-supervised losses, we further devise a novel ordinal distillation loss which aims to transfer the depth ordering information from a teacher model into our target model. The intuition of ordinal distillation is that the teacher model [27, 28] is usually good at predicting the depth ordering relationships of pixels (*e.g.*, a certain pixel is closer or farther than other pixels), albeit not reflecting the exact 3D geometry. Our final depth model becomes more robust and accurate by (i) learning the ordering relationships of all pixels via ordinal distillation and (ii) respecting the 3D geometry enforced by the photometric loss.

To perform quantitative evaluation, we collect a new dataset which contains stereo image sequences captured by a pair of stereo fisheye cameras mounted on an AR-Glasses device, and generate the pseudo groundtruth depth maps using stereo matching [44]. On this dataset, we show that our proposed model leads to significant improvements over the baseline models.

## 2 Related Work

In this section, we briefly review a few related works on self-supervised and supervised monocular depth estimation.

### Self-Supervised Depth Estimation

Most of self-supervised depth estimation methods assume that the camera is calibrated and the images are rectified such that a photometric loss can be constructed via a combination of unprojection and projection operations. Garg *et al.* [1] are the first to leverage the photo-consistency between stereo images to build a self-supervised loss for training a deep depth

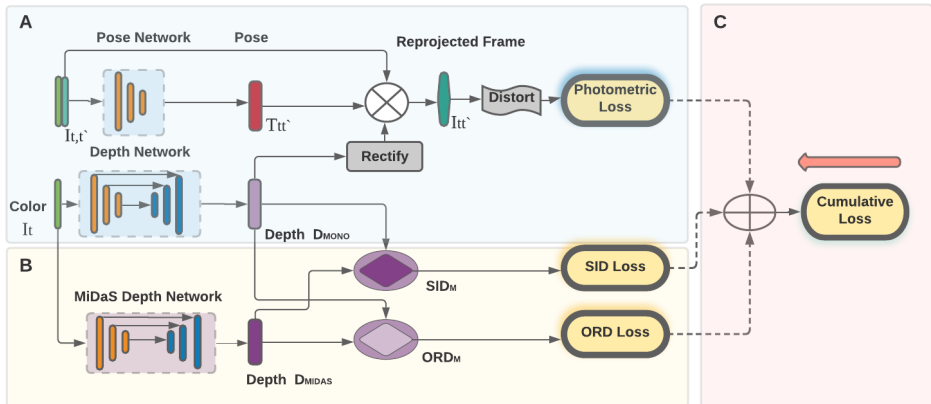


Figure 1: The system workflow of our **FisheyeDistill**. Our system consists of two main parts, *i.e.*, a student model trained with self-supervised losses and distillation losses, and a teacher model (MiDaS) [27, 28] that predicts depths to guide the training of the student model. The SID stands for the scale-invariant distillation and  $SID_M$  is the corresponding function module described in Sec. 3.3. ORD and  $ORD_M$  are the ordinal distillation loss and the module.

model. Zhou *et al.* [40] extend to using temporal sequences to train a depth model and a pose model with a temporal photometric loss. A lot of follow-up methods are then proposed to improve [9, 40] by new losses. Depth consistency losses are introduced to enforce the network to predict consistent depth maps in stereo [9] or temporal [10, 23] images. Wang *et al.* [53] observe a scale diminishing issue in monocular training and propose a depth normalization method to counter this issue. A few methods [54, 42] employ recurrent neural networks to model long-term temporal dependencies for self-supervised training. Some other methods [3, 37, 41] introduce an additional optical flow network to build cross-task consistencies in a monocular training setup. Godard *et al.* [11] comprehensively analyze the challenges faced in self-supervised depth learning, including occlusion, static pixels, and texture-copying artifacts, and propose a set of novel techniques to handle those challenges. Tiwari *et al.* [51] propose to combine self-supervised depth and geometric SLAM in a self-improving loop. Ji *et al.* [16] observe the challenges for indoor self-supervised depth estimation and come up with a depth factorization module and a residual pose estimation module to improve the performance under indoor environments. Watson *et al.* [59] use multiple temporal images as input to the depth model and put forth a teacher-student framework to deal with moving objects in the scene. Ji *et al.* [17] propose an online system for refining a depth model in a self-supervised manner, combining a robustified SLAM system and a monocular depth model.

## Supervised Depth Estimation

Ever since EigenDepth [9], many methods have been proposed to improve supervised monocular depth estimation on a specific dataset, either by using better loss terms [6, 22] or via multi-task learning [11, 25, 26, 30, 52, 59]. Instead of focusing on the depth prediction of one single dataset (or domain), some other methods seek to train a depth model that can learn

across different domains. Along this line, Megadepth [20] exploits internet photos to train a depth model with structure-from-motion reconstructions [29]. Li *et al.* [21] leverage internet videos with frozen people to predict sharp depth maps for images with people. MiDaS [27] proposes a scale-invariant loss to train the depth model on a large and diverse training sets, which facilitates generality and cross-dataset learning by providing a dataset-agnostic depth model. DPT [28] further improves MiDaS by using a vision transformer network [9]. Although visually pleasing depth maps can be generated by those models [27, 28], their quantitative performance on a specific dataset is usually worse than those that are trained specifically on the same dataset. This means that the accurate 3D geometry information is not well preserved in those models [27, 28].

Our method tries to reap the benefits of both self-supervised and supervised models in the sense that it respects the 3D geometry via the use of self-supervised losses and enforces ordering consistency between neighboring depth pixels by distilling information from a diversely trained teacher model.

### 3 Method

In this work, we aim at learning a self-supervised monocular depth estimation model for fisheye images (see Fig. 1). In all the previous works [4, 10, 11], view synthesis is usually used in self-supervision by learning a depth and pose relationship to synthesize virtual target images from neighboring views  $I_{t-1}$  and  $I_{t+1}$ . For this, it requires a projection function  $\Phi$  that maps 3D points  $P_i$  in 3D space to image coordinates  $p_i = \Phi(P_i)$ , and accordingly the corresponding unprojection function  $\Phi^{-1}$ , which converts image pixels, based on the estimated depth map  $D$ , into 3D space  $P_i = \Phi^{-1}(p_i, D)$  in order to acquire color information from other views.

#### 3.1 Fisheye Geometry Model

For fisheye cameras, given a 3D point  $P_i = (X_i, Y_i, Z_i)^T$  in camera coordinates and with  $(x_i = X_i/Z_i, y_i = Y_i/Z_i)$ , the projection function  $p_i = \Phi(P_i)$  from 3D point  $P_i$  to distorted image pixel  $p_i = (u, v)^T$  can be obtained through the following mapping equation:

$$\Phi(P_i) = \begin{cases} u = f_x \cdot x_d + c_x \\ v = f_y \cdot y_d + c_y \end{cases}, \quad (1)$$

where  $(x_d = \frac{x_i}{r} \phi_\theta, y_d = \frac{y_i}{r} \phi_\theta)$  with  $r = \sqrt{x_i^2 + y_i^2}$ ,  $\theta = \arctan(r)$  is the angle of incidence,  $\phi_\theta = \theta \cdot (1 + k_1 \cdot \theta^2 + k_2 \cdot \theta^4 + k_3 \cdot \theta^6 + k_4 \cdot \theta^8)$  is the polynomial radial distortion model mapping the incident angle to the image radius,  $(f_x, f_y)$  and  $(c_x, c_y)$  stand for the focal length and the principal point derived from the intrinsic matrix  $K$ , and  $\{k_i\}$  denote the set of fisheye distortion coefficients.

For the unprojection part, due to the existence of fisheye distortion, we are unable to directly transform a pixel  $p_i$  into camera coordinates via the pinhole model. In order to achieve that, we first generate an intermediate rectified depth map  $\hat{D}$  from the depth map  $D$  estimated from our network. This can be done by warping a pixel grid according to Eq. (1). Then we leverage the rectified  $\hat{D}$  to unproject the grid into 3D by simply applying  $\Phi^{-1}(p_i, \hat{D}) = \hat{D}K^{-1} \cdot p_i$ .<sup>1</sup> The view synthesis process in our fisheye pipeline can be

<sup>1</sup>Here and below, we omit a necessary step of converting to the homogeneous coordinates for notation simplicity.

summarized as: (i) Unproject a uniform pixel grid which has the same resolution with input frames through  $\Phi^{-1}(p_i, \hat{D})$ ; (ii) Project those 3D points by  $\Phi(P_i)$  and the associated pose information from pose network module, to obtain distorted synthesis images. This process is different from the FisheyeDistanceNet [18] which needs to numerically calculate  $\theta$  out from the 4<sup>th</sup> order polynomial.

### 3.2 Self-Supervised Losses

Following [10], we use a photometric reprojection loss between two neighboring fisheye images and an edge-aware depth smoothness loss as the self-supervised losses to train the models. Specifically, given a target fisheye image  $I_t$  and a source fisheye image  $I_{t'}$ , two models (*i.e.*, a depth model and a pose model) are jointly trained to predict a dense depth map  $D_t$  and a relative transformation matrix  $T_{t'}$ . The per-pixel minimum photometric reprojection loss [10] can be computed as

$$L^{ph} = \min_{t'} \rho(I_t, I_{t'}), \quad (2)$$

and

$$I_{t'} = I_{t'} \langle \Phi(T_{t'} \Phi^{-1}(p_i, \hat{D})) \rangle, \quad (3)$$

where  $t' \in \{t-1, t+1\}$ ,  $\rho(\cdot)$  denotes a weighted combination of the L1 and Structured SIMilarity (SSIM) losses [10], and  $\langle \cdot \rangle$  is the bilinear sampling operator. The edge-aware smoothness loss is defined as

$$L^{sm} = |\partial_x d_t^*| e^{-|\partial_x d_t|} + |\partial_y d_t^*| e^{-|\partial_y d_t|}, \quad (4)$$

where  $d_t^* = d/\bar{d}_t$  is the mean-normalized inverse depth from [13]. An auto-masking mechanism [10] is also adopted to mask out static pixels when computing the photometric loss.

### 3.3 Distillation Losses

Self-supervised losses are volatile when the brightness or RGB values of a pixel become indistinguishable with its neighboring pixels. Previously, such color ambiguity is implicitly handled via the smoothness loss and a multi-scale strategy [10], but they do not work well if the textureless regions are large. For example, in indoor environments, textureless walls often occupy a large area in the image; or in low-light/over-exposure conditions, most of the regions in an image are near-textureless. To provide supervision in those scenarios, we apply knowledge distillation [13] to distill depth information from a diversely trained teacher model [27, 28] into a smaller target model. In particular, we propose to combine a novel depth ordinal distillation loss and a scale-invariant distillation loss [27], which we detail as below.

Pretrained models such as MiDaS [27, 28] are good at predicting relative depth relationships as they are trained on large and diverse datasets. In light of this, we aim to distill from the teacher model the ordinal information between neighboring pixels into our student model. Inspired by [2], we propose to use a ranking loss to build an ordinal distillation loss between the depth maps from the teacher model and the target student model.

Given a depth map  $D^{MONO}$  from the student model and a depth map  $D^{MIDAS}$  from the teacher model, we compute a ranking loss from each pixel  $I(i, j)$  to its left neighbor  $I(i-1, j)$

as follows,

$$L_l^{od} = \begin{cases} \log(1 + \exp(-D_{i,j}^{MONO} + D_{i-1,j}^{MONO})), & \text{if } D_{i,j}^{MIDAS} > \alpha D_{i-1,j}^{MIDAS} \\ \log(1 + \exp(D_{i,j}^{MONO} - D_{i-1,j}^{MONO})), & \text{if } D_{i,j}^{MIDAS} < \beta D_{i-1,j}^{MIDAS} \\ |D_{i,j}^{MONO} - D_{i-1,j}^{MONO}|, & \text{otherwise,} \end{cases} \quad (5)$$

where  $\alpha$  and  $\beta$  are hyper-parameters controlling the ranking gap and are empirically set to  $\alpha = 1.1$  and  $\beta = 0.9$  in our experiments. Similarly, we can compute a ranking loss from each pixel  $I(i, j)$  to its neighbor above it:  $I(i, j - 1)$  as  $L_t^{od}$ . The final ordinal distillation loss is then the sum of  $L_l^{od}$  and  $L_t^{od}$ , *i.e.*,

$$L^{od} = L_l^{od} + L_t^{od}. \quad (6)$$

Intuitively, if a pixel is predicted to be farther (or closer) than its neighbors by the teacher model, by minimizing the ordinal distillation loss, the student model is encouraged to predict similar depth ordering relationships. If in the teacher model two neighboring pixels are predicted to be close, a smoothness term is enforced for the student model.

We further add a scale-invariant distillation loss  $L^{sd}$  between  $D^{MONO}$  and  $D^{MIDAS}$  to strengthen the supervision in textureless regions. Following [27],  $D^{MONO}$  and  $D^{MIDAS}$  are respectively normalized to be scale- and shift-invariant (subtracted by the median scale and then divided by the mean shift). The normalized versions are denoted as  $\tilde{D}^{MONO}$  and  $\tilde{D}^{MIDAS}$ . The scale-invariant loss is then defined as:

$$L^{sd} = |\tilde{D}^{MONO} - \tilde{D}^{MIDAS}|. \quad (7)$$

Our final training loss is a weighted combination of the photometric loss, the smoothness loss and the distillation losses, *i.e.*,

$$L = L^{ph} + w^{sm} L^{sm} + w^{od} L^{od} + w^{sd} L^{sd}. \quad (8)$$

## 4 AR-Glasses Fisheye Dataset

In order to evaluate the model, we contribute a large fisheye dataset for training and evaluation. The dataset contains 321,300 raw fisheye images collected from a well calibrated AR-Glasses device in a stereo manner. All images are acquired in an indoor environment with 8 different scenes. Besides various chairs, desks and decorations, there are also many lights, texture-less walls and glasses therein. In addition, due to the computational limit on the headset, all frames are captured under the resolution of  $640 \times 400$  in gray-scale with a sub-optimal auto-exposure mechanism. These make our dataset very challenging for the task of self-supervised depth estimation as the photometric constraints would act poorly in such scenes. We will have more discussion on it in Sec. 5.2.

More specifically, in our experiments, we use 238,186 images for training and 42,688 and 20,213 images as the validation and test sets respectively. The 8 scenarios are randomly shuffled and fed into the network while training. Similar to [10], we also apply the static frame filtering to clean our data and get a final training and a validation set of 71,688 and 6,265 images. One major limitation of other fisheye datasets [24] is that there is no easily accessible ground truth for evaluation. Instead, we utilize the semi-global stereo matching method [14] based on OpenCV's implementation to calculate pseudo ground truth for our dataset. In our experiments, we select 300 well calculated stereo depth maps from different viewpoints as ground truth. We conduct all the experiments in the monocular mode.

## 5 Experiments

### 5.1 Implementation Details

We implement our system using Pytorch and employ Adam optimizer to minimize the objective function in Eq. (8). We train the model for 20 epochs with a learning rate of  $10^{-4}$  on a 12GB GeForce RTX. Due to the limitation of graphic memory, a small batch size of 6 is leveraged while training and batch normalization [14] layers are also frozen to avoid unexpected degeneration. We convert the sigmoid output  $\sigma$  from the network to depth via  $D = 1/(a \cdot \sigma + b)$ , where  $a$  and  $b$  are chosen to bound  $D$  between 0.1 and 100 units. As the resolution of our AR-Glasses images is  $640 \times 400$ , we feed  $640 \times 384$  pixels as the network input to approximate the original aspect ratio. The smoothness loss weight  $w^{sm}$  is set to  $10^{-3}$  and distillation loss weights  $w^{od} = w^{sd} = 1.0$ . For generating the rectified intermediate depth  $\hat{D}$ , we apply a slightly small focal length than the one given in  $K$ . This would help the network to better learn the content on distorted image boundaries. In all our experiments, we use 0.8 as the scale factor.

As previously discussed, while the MiDaS teacher model [28] provides a good guidance for depth estimation even on challenging structures, it suffers from the limitation in keeping true geometric relationship, due to the lack of cross-view photometric constraints. Therefore, directly adopting a constant weight for the knowledge distillation through all epochs would weaken the ability of learning better geometry information. To circumvent this issue, we adopt a decay weighting strategy for the distillation losses in training. After each  $10k$  steps, we decay the weights  $w^{od}$  and  $w^{sd}$  by applying a factor  $s = 0.9^{2\lambda}$ , where  $\lambda = \frac{steps}{10000}$ . Such a strategy enables a major contribution from the distillation losses when the uncertainty is high and facilitates the convergence of photometric constraints in the later training stage. After five epochs, photometric losses begin to play a more dominant role in model training, which ensures the acquisition of geometric relationship between temporal frames. Similar to other self-supervised works, we also set the length of the training snippets to 3 and build the losses over 4 image scales.

### 5.2 Evaluation

We evaluate our model mainly on the proposed AR-Glasses fisheye dataset. We do not leverage KITTI [8] as it is not a fisheye dataset. Woodscape [18] dataset could be a good candidate, but it is still not fully released. Currently only around  $8k$  images are available and without ground truth for evaluation. While the image resolution of AR-Glasses dataset is smaller than KITTI dataset, the ground truth is much denser. Moreover, since there is no explicit sky region in the indoor environment, we do not perform any cropping for each test image. We evaluate the models on all pixels whose depth values are not zero in the computed groundtruth.

The quantitative results are reported in Table 5.2, which shows the performance of our model on the AR-Glasses dataset. From the table, we can see that without considering the fisheye distortion, Monodepth2 [11] is unable to extract plausible depth outputs from distorted images. MiDaS [28] shows a good generalization ability on our dataset, despite being trained on rectified images. We are unable to compare with the fisheye model [18], as its source code is not publicly available. As fisheye cameras are designed for near-field sensing and deployed on AR-Glasses for indoor applications, the groundtruth depth values are capped at  $20m$  for evaluation. In addition, we also demonstrate how the decay factor  $s$

Table 1: Quantitative results of different algorithms on AR-Glasses fisheye dataset. All the approaches are evaluated in the monocular mode and the estimated depths are scaled using median scaling.

Method	Abs Rel	Sq Rel	RMSE	RMSE_log	$\delta < 1.25$	$\delta < 1.25^2$	$\delta < 1.25^3$
Monodepth2 [11]	0.348	0.108	0.198	0.398	0.449	0.749	0.895
MiDaS [23]	0.216	0.131	0.252	0.267	0.756	0.918	0.965
Ours with $s = 0.98^{2\lambda}$	0.136	0.022	0.103	0.183	0.843	0.971	0.991
Ours with $s = 0.9^{2\lambda}$	0.131	0.020	0.098	0.177	0.854	0.973	0.992

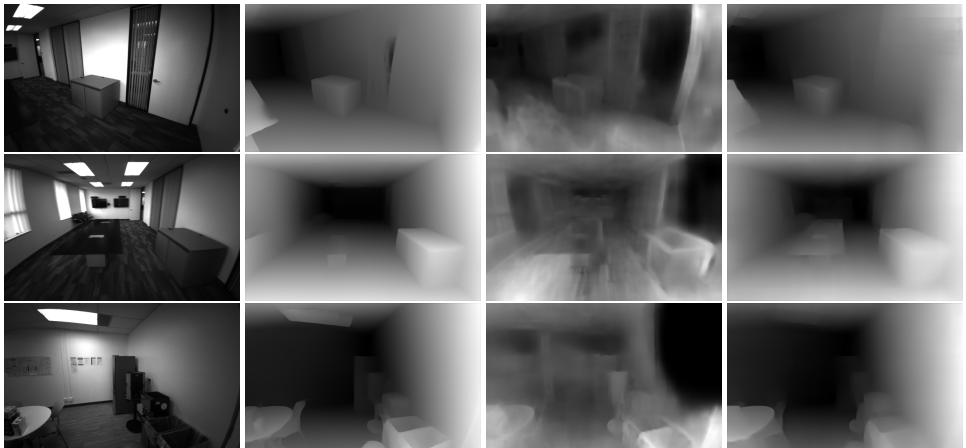


Figure 2: Qualitative results on the AR-Glasses dataset. From left to right, the images are respectively input fisheye images, MiDaS estimated disparity maps, disparity maps from our network without any distillation losses, and disparity maps with distillation losses.

affects the performance in training. We report the comparison results by employing  $s = 0.9^{2\lambda}$  and  $\hat{s} = 0.98^{2\lambda}$  respectively, where  $\hat{s}$  enforces more emphasis on the distillation part. It can be found that letting the network learn more geometric information through the temporal photometric loss helps to improve the results.

We also render the qualitative results to demonstrate our advantages in challenging indoor environments, as shown in Fig. 4. Directly training upon photometric constraints without knowledge distillation is prone to producing halo and texture-copy artifacts. This is because that large texture-less continuous surfaces, such as planar white walls and desks, and the low light condition make photometric losses unable to well establish pixel correspondences from the very beginning. In contrast, due to the good generalization ability on different datasets, the MiDaS teacher model [23], provides a smooth and sharp depth ordering hint to let the network approximate plausible depth even on texture-less planes. However, the geometric constraint within MiDaS is insufficient. This is notable from Fig. 3, where we visualize the 3D geometry unprojected from corresponding depth maps of different methods. While the depth map is visually-pleasant, MiDaS suffers from severe distortion in 3D space. Our method overcomes the limitations existing in both [11] and [23] and is able to give more consistent results on the challenging indoor dataset.



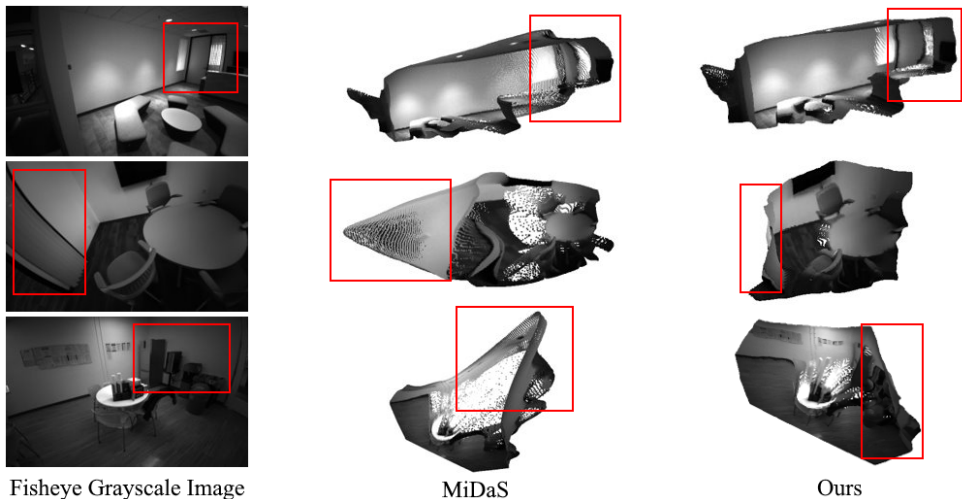


Figure 3: Visual comparison of the 3D point clouds generated from depth maps by MiDaS (middle) and our method (right). Compared to MiDaS, our results generate more geometrically correct point clouds.

Table 2: Ablation study by using different variants on the proposed AR-Glasses dataset. Depths are all capped at  $20m$ . SID, ORD, DW respectively represent the scale-invariant distillation, ordinal distillation and decay weighting.

Method	SID	ORD	DW	Abs Rel	Sq Rel	RMSE	RMSE_log	$\delta < 1.25$	$\delta < 1.25^2$	$\delta < 1.25^3$
Ours	✗	✗	✗	0.151	0.021	0.103	0.200	0.780	0.961	0.992
Ours	✓	✓	✗	0.134	0.020	0.098	0.180	0.846	0.972	0.992
Ours	✓	✗	✓	0.134	0.019	0.097	0.179	0.844	0.972	0.992
Ours	✓	✓	✓	0.131	0.020	0.098	0.177	0.854	0.973	0.992

### 5.3 Ablation Study

We conduct an ablation study to illustrate the benefits of different components used in our system and show the results in Table 5.2. (i) Remove both distillation losses: The network is trained only with distortion-based self-supervised photometric losses. As previously discussed, the proposed AR-Glasses dataset is very challenging, due to under-exposure and textureless structures. Only relying on photometric constraints is prone to producing halo and texture-copy artifacts. In contrast, the distillation strategy offers a huge quantitative improvement. Fig. 3 also provides a visual comparison for the sake of illustration. (ii) Remove the ordinal distillation loss: Ordinal distillation loss is good at the supervision in textureless regions. Removing the ordinal distillation loss from the network would diminish the performance gain over the baseline. (iii) Utilize constant distillation loss weights: Apart from the comparison of using different  $s$  as illustrated before, we also launch an experiment with a constant distillation weighting strategy. For the trade-off between keeping depth ordering and learning true geometry, we set the loss weights to  $w^{od} = w^{sd} = 0.3$  without decaying here for testing. It can be seen that using constant distillation loss weights decrease the performance on our dataset, which verifies the effectiveness of our decay-weighting strategy.

## 6 Conclusions

In this work, we have presented FisheyeDistill, a self-supervised monocular depth estimation method for fisheye cameras. Our key insight is to combine self-supervised fisheye photometric losses with a novel ordinal distillation loss to train a robust depth model that can work well in challenging environments for fisheye cameras.

## Appendix

We adopt the same network structures with [10]. In all experiments we use a standard ResNet18 [12] encoder for both depth and pose networks. The pose encoder takes fisheye frames as input, as our network is trained to learn the pose under the distortion circumstance. We also empirically found that using corresponding rectified images as input to the pose network decreases its performance. For the distillation part, we leverage the pretrained DPT [28] large model as our teacher model. For further demonstration, we also upload a demo video, which respectively shows a portion of our contributed AR-glass fisheye dataset and the corresponding depth estimation results (with and without knowledge distillation). It is evident that without the proposed distillation strategies, the results suffer from significant halo artifacts, as is also shown below.

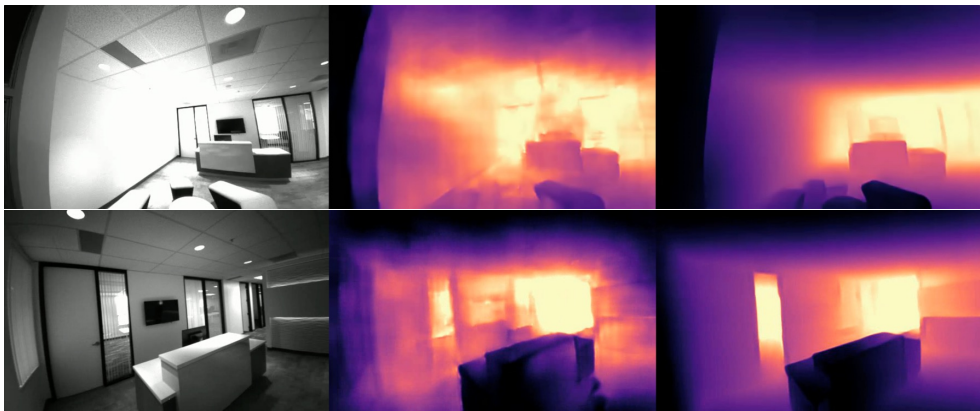


Figure 4: Depth estimation results on the AR-Glasses dataset. From left to right are respectively the fisheye frames in our dataset, and the color-coded depth predictions from our network without and with using the proposed distillation strategies.

## References

- [1] Jia-Wang Bian, Zhichao Li, Naiyan Wang, Huangying Zhan, Chunhua Shen, Ming-Ming Cheng, and Ian Reid. Unsupervised scale-consistent depth and ego-motion learning from monocular video. *arXiv preprint arXiv:1908.10553*, 2019.
- [2] Weifeng Chen, Zhao Fu, Dawei Yang, and Jia Deng. Single-image depth perception in the wild. *arXiv preprint arXiv:1604.03901*, 2016.

- [3] Yuhua Chen, Cordelia Schmid, and Cristian Sminchisescu. Self-supervised learning with geometric constraints in monocular video: Connecting flow, depth, and camera. In *Proceedings of the IEEE/CVF International Conference on Computer Vision*, pages 7063–7072, 2019.
- [4] Alexey Dosovitskiy, Lucas Beyer, Alexander Kolesnikov, Dirk Weissenborn, Xiaohua Zhai, Thomas Unterthiner, Mostafa Dehghani, Matthias Minderer, Georg Heigold, Sylvain Gelly, et al. An image is worth 16x16 words: Transformers for image recognition at scale. *arXiv preprint arXiv:2010.11929*, 2020.
- [5] David Eigen, Christian Puhrsch, and Rob Fergus. Depth map prediction from a single image using a multi-scale deep network. *arXiv preprint arXiv:1406.2283*, 2014.
- [6] Huan Fu, Mingming Gong, Chaohui Wang, Kayhan Batmanghelich, and Dacheng Tao. Deep ordinal regression network for monocular depth estimation. In *CVPR*, pages 2002–2011, 2018.
- [7] Ravi Garg, Vijay Kumar Bg, Gustavo Carneiro, and Ian Reid. Unsupervised cnn for single view depth estimation: Geometry to the rescue. In *ECCV*, pages 740–756, 2016.
- [8] Andreas Geiger, Philip Lenz, Christoph Stiller, and Raquel Urtasun. Vision meets robotics: The kitti dataset. *The International Journal of Robotics Research*, 32(11): 1231–1237, 2013.
- [9] Clément Godard, Oisín Mac Aodha, and Gabriel J Brostow. Unsupervised monocular depth estimation with left-right consistency. In *CVPR*, pages 270–279, 2017.
- [10] Clément Godard, Oisín Mac Aodha, Michael Firman, and Gabriel J Brostow. Digging into self-supervised monocular depth estimation. In *ICCV*, pages 3828–3838, 2019.
- [11] Xiaoyang Guo, Hongsheng Li, Shuai Yi, Jimmy Ren, and Xiaogang Wang. Learning monocular depth by distilling cross-domain stereo networks. In *ECCV*, pages 484–500, 2018.
- [12] Kaiming He, Xiangyu Zhang, Shaoqing Ren, and Jian Sun. Deep residual learning for image recognition. In *Proceedings of the IEEE conference on computer vision and pattern recognition*, pages 770–778, 2016.
- [13] Geoffrey Hinton, Oriol Vinyals, and Jeff Dean. Distilling the knowledge in a neural network. *arXiv preprint arXiv:1503.02531*, 2015.
- [14] Heiko Hirschmüller. Stereo processing by semiglobal matching and mutual information. *TPAMI*, 30(2):328–341, 2007.
- [15] Sergey Ioffe and Christian Szegedy. Batch normalization: Accelerating deep network training by reducing internal covariate shift. In *ICML*, pages 448–456. PMLR, 2015.
- [16] Pan Ji, Runze Li, Bir Bhanu, and Yi Xu. Monoindoor: Towards good practice of self-supervised monocular depth estimation for indoor environments. In *ICCV*, pages 12787–12796, 2021.
- [17] Pan Ji, Qingan Yan, Yuxin Ma, and Yi Xu. Georefine: Self-supervised online depth refinement for accurate dense mapping. *arXiv preprint arXiv:2205.01656*, 2022.

- [18] Varun Ravi Kumar, Sandesh Athni Hiremath, Markus Bach, Stefan Milz, Christian Witt, Clément Pinard, Senthil Yogamani, and Patrick Mäder. Fisheyedistancenet: Self-supervised scale-aware distance estimation using monocular fisheye camera for autonomous driving. In *ICRA*, pages 574–581, 2020.
- [19] Varun Ravi Kumar, Senthil Yogamani, Markus Bach, Christian Witt, Stefan Milz, and Patrick Mader. Unrectdepthnet: Self-supervised monocular depth estimation using a generic framework for handling common camera distortion models. *arXiv preprint arXiv:2007.06676*, 2020.
- [20] Zhengqi Li and Noah Snavely. Megadepth: Learning single-view depth prediction from internet photos. In *CVPR*, pages 2041–2050, 2018.
- [21] Zhengqi Li, Tali Dekel, Forrester Cole, Richard Tucker, Noah Snavely, Ce Liu, and William T Freeman. Learning the depths of moving people by watching frozen people. In *CVPR*, pages 4521–4530, 2019.
- [22] Fayao Liu, Chunhua Shen, Guosheng Lin, and Ian Reid. Learning depth from single monocular images using deep convolutional neural fields. *TPAMI*, 38(10):2024–2039, 2015.
- [23] Xuan Luo, Jia-Bin Huang, Richard Szeliski, Kevin Matzen, and Johannes Kopf. Consistent video depth estimation. *TOG*, 39(4):71–1, 2020.
- [24] Hidenobu Matsuki, Lukas von Stumberg, Vladyslav Usenko, Jörg Stückler, and Daniel Cremers. Omnidirectional dso: Direct sparse odometry with fisheye cameras. *IEEE Robotics and Automation Letters*, 3(4):3693–3700, 2018.
- [25] Xiaojuan Qi, Renjie Liao, Zhengzhe Liu, Raquel Urtasun, and Jiaya Jia. Geonet: Geometric neural network for joint depth and surface normal estimation. In *CVPR*, pages 283–291, 2018.
- [26] Siyuan Qiao, Yukun Zhu, Hartwig Adam, Alan Yuille, and Liang-Chieh Chen. Vip-deeplab: Learning visual perception with depth-aware video panoptic segmentation. In *CVPR*, pages 3997–4008, 2021.
- [27] René Ranftl, Katrin Lasinger, David Hafner, Konrad Schindler, and Vladlen Koltun. Towards robust monocular depth estimation: Mixing datasets for zero-shot cross-dataset transfer. *arXiv preprint arXiv:1907.01341*, 2019.
- [28] René Ranftl, Alexey Bochkovskiy, and Vladlen Koltun. Vision transformers for dense prediction. *arXiv preprint arXiv:2103.13413*, 2021.
- [29] Johannes L Schonberger and Jan-Michael Frahm. Structure-from-motion revisited. In *CVPR*, pages 4104–4113, 2016.
- [30] Zachary Teed and Jia Deng. Deepv2d: Video to depth with differentiable structure from motion. *arXiv preprint arXiv:1812.04605*, 2018.
- [31] Lokender Tiwari, Pan Ji, Quoc-Huy Tran, Bingbing Zhuang, Saket Anand, and Manmohan Chandraker. Pseudo rgb-d for self-improving monocular slam and depth prediction. In *ECCV*, pages 437–455, 2020.

- [32] Benjamin Ummenhofer, Huizhong Zhou, Jonas Uhrig, Nikolaus Mayer, Eddy Ilg, Alexey Dosovitskiy, and Thomas Brox. Demon: Depth and motion network for learning monocular stereo. In *CVPR*, pages 5038–5047, 2017.
- [33] Chaoyang Wang, José Miguel Buenaposada, Rui Zhu, and Simon Lucey. Learning depth from monocular videos using direct methods. In *CVPR*, pages 2022–2030, 2018.
- [34] Rui Wang, Stephen M Pizer, and Jan-Michael Frahm. Recurrent neural network for (un-) supervised learning of monocular video visual odometry and depth. In *CVPR*, pages 5555–5564, 2019.
- [35] Jamie Watson, Oisín Mac Aodha, Victor Prisacariu, Gabriel Brostow, and Michael Firman. The temporal opportunist: Self-supervised multi-frame monocular depth. In *CVPR*, pages 1164–1174, 2021.
- [36] Wei Yin, Jianming Zhang, Oliver Wang, Simon Niklaus, Long Mai, Simon Chen, and Chunhua Shen. Learning to recover 3d scene shape from a single image. In *CVPR*, pages 204–213, 2021.
- [37] Zhichao Yin and Jianping Shi. Geonet: Unsupervised learning of dense depth, optical flow and camera pose. In *CVPR*, pages 1983–1992, 2018.
- [38] Senthil Yogamani, Ciarán Hughes, Jonathan Horgan, Ganesh Sistu, Pádraig Varley, Derek O’Dea, Michal Uricár, Stefan Milz, Martin Simon, Karl Amende, et al. Woodscape: A multi-task, multi-camera fisheye dataset for autonomous driving. In *ICCV*, pages 9308–9318, 2019.
- [39] Huizhong Zhou, Benjamin Ummenhofer, and Thomas Brox. Deeptam: Deep tracking and mapping. In *ECCV*, pages 822–838, 2018.
- [40] Tinghui Zhou, Matthew Brown, Noah Snavely, and David G Lowe. Unsupervised learning of depth and ego-motion from video. In *CVPR*, pages 1851–1858, 2017.
- [41] Yulian Zou, Zelun Luo, and Jia-Bin Huang. DF-Net: Unsupervised joint learning of depth and flow using cross-task consistency. In *ECCV*, 2018.
- [42] Yulian Zou, Pan Ji, Quoc-Huy Tran, Jia-Bin Huang, and Manmohan Chandraker. Learning monocular visual odometry via self-supervised long-term modeling. *arXiv preprint arXiv:2007.10983*, 2020.